Experimental test of revised similarity hypotheses without Taylor's hypothesis

Duo Xu and Jun Chen*

School of Mechanical Engineering, Purdue University, 585 Purdue Mall, West Lafayette, Indiana 47906, USA

(Received 5 June 2012; published 24 January 2013)

The refined similarity hypotheses (RSH) and their extension to passive scalar (RSH-P) are tested experimentally using simultaneous velocity and scalar data in a turbulent jet. Different from the single-point hot-wire probe in a previous experimental test, a combined particle image velocimetry and planar laser induced fluorescence technique enable us to obtain the test data without applying Taylor's hypothesis. RSH is successfully validated with direct examinations of its three hypotheses. RSH-P is partially supported, where the hypothesis of independent behavior of the stochastic variable υ_θ is not supported. The conditional probability density functions (PDFs) of υ and υ_θ cannot be described by Gaussian distributions when $\mathrm{Re_r} < 5$ for υ and $\mathrm{Re_r} < 300$ for υ_θ, and their Gaussian peaks converge when $\mathrm{Re_r} > 100$ for υ and $\mathrm{Re_r} > 1000$ for υ_θ. In addition, the bimodal behavior of the PDFs and oscillations at small r in previous experimental tests are not observed in this study.

DOI: 10.1103/PhysRevE.87.013018 PACS number(s): 47.27.E−

I. INTRODUCTION

Inspired by Richardson's description of energy cascade [1], Kolmogorov [2] introduced that the anisotropic influence from the large scales would be lost during the breakdown of eddies and at the sufficiently small scales the flow would be statistically homogeneous and isotropic, which was proposed in the famous *Kolmogorov's similarity hypotheses* (K41) and believed as the era culmination of turbulent study [3]. K41 states that the statistics of the small-scale motions should have a universal form when the Reynolds number is sufficiently high. The nth moment of velocity increment, $\Delta u_r' \equiv u'(x+r) - u'(x)$, is related to the turbulent dissipation, $\epsilon = 2\nu s_{ij} s_{ij}$ [ν is the kinematic viscosity, and the strain rate tensor is $s_{ij} = 0.5(\partial u_i'/\partial x_j + \partial u_j'/\partial x_i)$], by

$$\left\langle \Delta u_r'^n \right\rangle = C_n (r\langle\epsilon\rangle)^{n/3}, \tag{1}$$

where $\langle\cdot\rangle$ denotes an averaging operation, and C_n is a universal constant and r is within the inertial subrange. However, for high orders $n \geqslant 4$, it is known that the discrepancies of scaling exponents exist between the predictions of the Kolmogorov theory (K41) and experimental results, where the deviations are known as anomalous scaling [4]. This phenomenon is termed *intermittency*. To account for intermittency, Kolmogorov [5] and Oboukhov [6] revised K41 to *refined similarity hypotheses* (RSH): (1) Δu_r is related to a local energy dissipation rate

$$\epsilon_r \equiv \frac{1}{V}\int \epsilon(\mathbf{x}) d\mathbf{x}, \tag{2}$$

where V is a volume of linear dimension r, instead of $\langle\epsilon\rangle$, by

$$\Delta \mathbf{u}_\mathbf{r}' = \upsilon(\mathbf{r}\epsilon_r)^{1/3}. \tag{3}$$

Here the nondimensional stochastic variable υ is independent of r and ϵ_r. (2) The probability density function (PDF) of υ, $P(\upsilon)$, varies with a local Reynolds number

$$\mathrm{Re_r} = r(r\epsilon_r)^{1/3}/\nu, \tag{4}$$

when $r \ll L$ (L is integral length scale). (3) Furthermore, when $\mathrm{Re_r} \gg 1$, $P(\upsilon)$ is independent of $\mathrm{Re_r}$ [5,6].

Previously, extensive efforts have been drawn to validate RSH. Since all nine elements of s_{ij} cannot be fully measured in experiments, a certain surrogate of ϵ using measurable components must be adopted in the analysis, such as $\epsilon \simeq 15\nu(\partial u_1'/\partial x_1)^2$, by assuming isotropy. Hosokawa and Yamamoto [7,8] discovered evidence against RSH by using a direct numerical simulation (DNS) on isotropic turbulence, while other studies, using DNS and high-Reynolds number laboratory and atmospheric experiments, tend to support RSH [9–13]. Hot-wire measurement of a cylinder wake at a Taylor scale Reynolds number $R_\lambda = 533$ shows a joint probability density function (JPDF) of Δu_r and $(r\epsilon_r)^{1/3}$ depends on r in the inertial subrange [11]. Analysis of the correlation between $|\Delta u_r|$ and ϵ_r has been applied to test RSH using experimental data [10] and DNS data [12]. However, the correlation coefficient decreases as r increases in the inertial subrange, which is less supportive to the hypotheses [10].

In wind tunnel experiments using hot-wire measurements, when ϵ is estimated by the streamwise gradient of the transverse velocity component $\epsilon \simeq 7.5\nu(\partial u_3'/\partial x_1)^2$ (transverse surrogate) instead of the commonly used $\epsilon \simeq 15\nu(\partial u_1'/\partial x_1)^2$ (longitudinal surrogate), the dependence between $|\Delta u_r'|$ and $(r\epsilon_r)^{1/3}$ disappears (correlation coefficient $\sim$0.1), and this suggests that the previous experimental support for RSH may be premature [14]. A study using DNS leads to a similar conclusion [15]. To respond to this finding, Praskovasky *et al.* experimentally tested RSH in a mixing layer generated in a wind tunnel at high Reynolds number ($R_\lambda > 10^3$), and showed that both the transverse surrogate and longitudinal surrogate led to higher correlations between $|\Delta u_r'|$ and $(r\epsilon_r)^{1/3}$ than the result in Ref. [14], thus RSH is still valid [16]. Hosokawa *et al.* [17] showed that one-dimensional surrogates of ϵ gain more intermittency, which can introduce fundamental changes in the statistics of turbulence. A systematic study of the intermittent behavior using DNS data reveals that all surrogates of ϵ are more intermittent than the true dissipation (analyzed using all nine elements of s_{ij}), especially for the transverse surrogate [18]. This work suggests that as many measurable elements of s_{ij} should be used in estimating ϵ in order to reduce the overintermittent behavior [18].

RSH has also been extended into the passive scalar field (RSH-P) by assuming that velocity u and scalar θ are

*junchen@purdue.edu

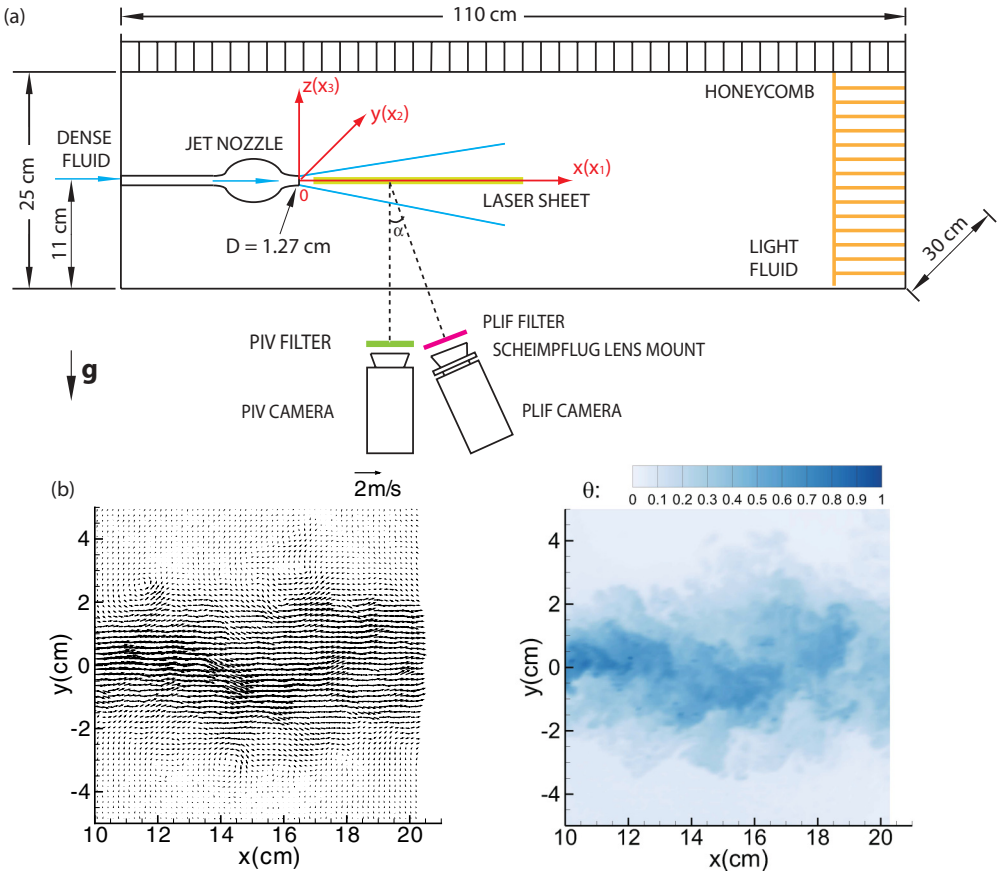

FIG. 1. (Color online) (a) Schematics of the turbulent jet facility, and a snapshot of simultaneous velocity (b) and scalar (c) fields. Only 1/4 of the velocity vectors are plotted for clarity of display.

equivalent to a certain extent in the inertial subrange [19,20]. In particular,

$$\Delta\theta'_r \equiv \theta'(x+r) - \theta'(x) = \upsilon_\theta\left(r^{1/3}\epsilon_r^{-1/6}\chi_r^{1/2}\right), \qquad (5)$$

where

$$\chi_r \equiv \frac{1}{V}\int \chi(\mathbf{x})d\mathbf{x} \qquad (6)$$

is a local averaged scalar dissipation, and

$$\chi \equiv 2\Gamma \frac{\partial\theta'}{\partial x_j}\frac{\partial\theta'}{\partial x_j}, \qquad (7)$$

where Γ is the diffusivity, and $\theta' = \theta - \langle\theta\rangle$. Similar to RSH, RSH-P states the following: (1) The nondimensional stochastic variable υ_θ is independent of r, ϵ_r, and χ_r; (2) when $r \ll L$, the PDF of υ_θ, $P(\upsilon_\theta)$, varies with $\mathrm{Re_r}$; and (3) when $\mathrm{Re_r} \gg 1$, $P(\upsilon_\theta)$ is independent of $\mathrm{Re_r}$. Among a few experiments, hot-cold wire measurements of a circular jet and a cylinder wake in wind tunnels support RSH-P [21,22]. The dynamical aspect of RSH-P was tested using DNS and the obtained $P(\upsilon_\theta)$ is nearly Gaussian [23].

When DNS is applied to test RSH and RSH-P, different studies lead to different conclusions [7,8,12], and the boundary conditions of DNS are usually idealized (e.g., periodic boundary condition). Other dominant contributions for testing RSH and RSH-P were from the hot-cold-wire probe measurements in a wind tunnel. When a hot-wire (or a hot-cold-wire) probe is applied in the experiments, Taylor's hypothesis has to be adopted to extract spatial statistics from pointwise temporal measurements. But to measure the small-scale derivatives of velocity (or scalar), the results invoking Taylor's hypothesis introduce possible errors, i.e., derivatives from Taylor's hypothesis yield a correlation ranging from 0.56 to 0.74 with the true values (see the details in Ref. [24]). A recent numerical simulation study interprets the bimodal spectra derived from channel flow as artifacts of Taylor's hypothesis [25,26], which evokes doubt as to whether Taylor's hypothesis brings in artifacts to the test of RSH (and RSH-P). In addition, the single-probe application measuring ϵ leads to premature test conclusions by using a one-dimensional surrogate [14,15]. When the hot-cold-wire probe is applied, the cold-wire probe (mounted in front of the hot-wire probe) introduces possible interference to the velocity measuring of the hot-wire probe, since the distance between the two probes is small (i.e., $2\eta_k - 3\eta_k$ in Refs. [21,27]).

Yeung *et al.* [28] and Ishihara *et al.* [29,30] suggest the moderate-Reynolds-number simulation could exhibit high-Reynolds-number flow characteristics, which also should be suitable to experimental work. Hence, in this paper, we present an independent laboratory experimental test of RSH and RSH-P using simultaneously measured high-resolution velocity-scalar data from a turbulent jet. The velocity data within the two-dimensional (2D) measurement plane were measured using particle image velocimetry (PIV), whereas the scalar

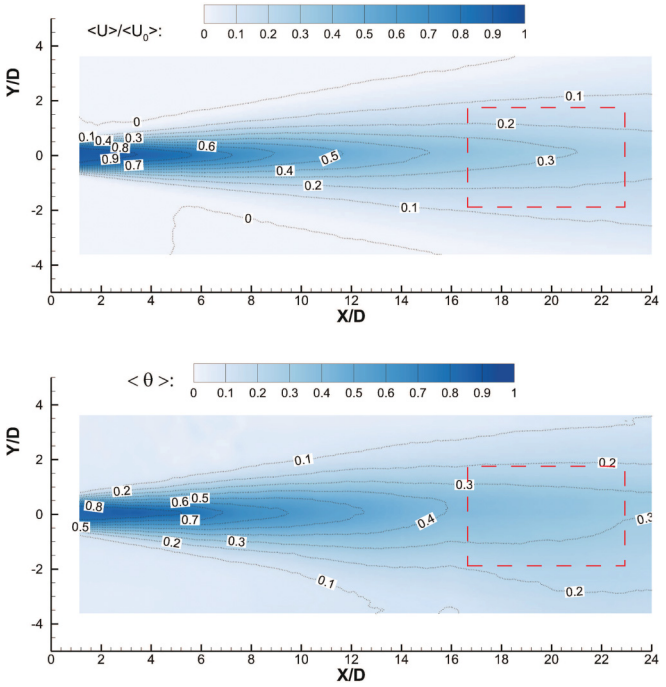

FIG. 2. (Color online) (a) Mean nondimensional streamwise velocity $\langle U\rangle/\langle U_0\rangle$ and (b) mean nondimensional density difference $\langle\theta\rangle$ distribution. The red dashed rectangular indicates the data used in this study.

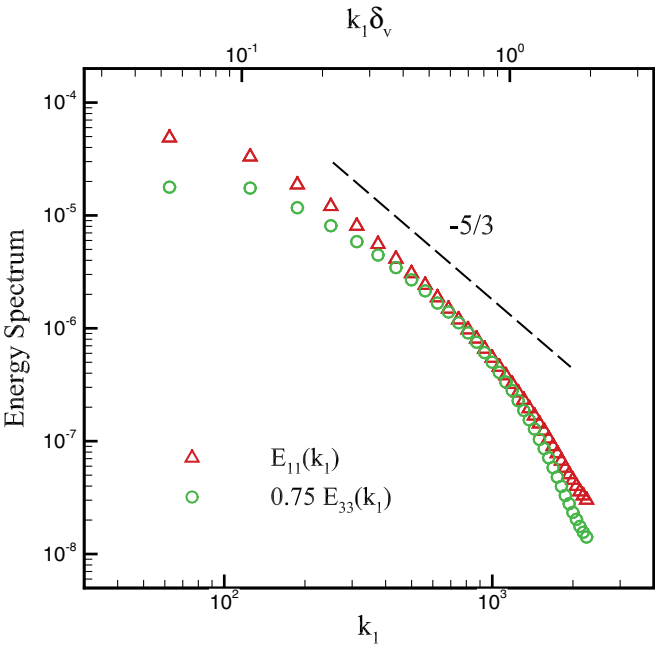

FIG. 3. (Color online) energy spectra $E_{11}(k_1)$ and $E_{33}(k_1)$.

data were obtained using planar laser induced fluorescence (PLIF). These field measurements enable us to revisit RSH and RSH-P without Taylor's hypothesis. Our main result is that RSH is successfully validated through direct testing of the hypotheses, and the trend of variation of $P(\upsilon)$ and its approach to being uniform is clearly observed when $\mathrm{Re_r}$ increases. While the similar trend of variation of $P(\upsilon_\theta)$ and its approach to being uniform is also observed when $\mathrm{Re_r}$ increases, however, the independence of υ_θ on r, ϵ_r, and χ_r is not observed.

II. EXPERIMENT

The experiment setup, sketched in Fig. 1 and described in detail in Ref. [31], consists of a dense fluid (density ρ_s, mixed with fluorescent dye) horizontally injected through a nozzle into light fluid (ρ_e) with a slight density difference (as shown in Table I). The details of the experimental running condition are shown in Table I. In the experiments, the bulk Richardson number $\mathrm{Ri_b} = 0.0002$, thus the influence of stratification is minimal. The overlap region of $E_{11}(k_1)$ and $0.75E_{33}(k_1)$ in Fig. 3 indicates the inertial subrange, which is conservatively estimated as $15\delta_v - 35\delta_v$ (see e.g., Ref. [4]).

A 1/2-mm-thick laser sheet was formed through a group of lenses to illuminate a horizontal plane $(x-y)$ at $z = 0$. A combined PIV-PLIF technique was developed to simultaneously measure the velocity and density (scalar) fields. The scalar field from PLIF ($\Delta_\theta = 0.054$ mm) is sampled to match the resolution of the velocity field from the PIV measurement ($\Delta_v = 0.86$ mm). More details of the technique and calibration can be found in Ref. [31], and the uncertainties of instantaneous measurements are 0.7% for velocity and 2% for scalar. Three

TABLE I. Experimental conditions. Local values are computed using data from the area of interest enclosed by red dashed lines in Fig. 2.

Parameter	Value
Inlet velocity $\langle U_0\rangle$	1.9 m/s
Inlet density difference $\Delta\rho_0/\rho_s = (\rho_s - \rho_e)/\rho_s$	0.5%
Fluctuation ratio $u_{\mathrm{rms}}/v_{\mathrm{rms}}$	1.15
Turbulent intensity $u_{\mathrm{rms}}/\langle U_0\rangle$	4.5%
Inlet Reynolds number $\mathrm{Re_0} = \langle U_0\rangle D/\nu$	24 000
Inlet Taylor scale Reynolds number R_λ	265
Inlet bulk Richardson number $\mathrm{Ri_b} = \Delta\rho_0 Dg/(\rho_s\langle U_0\rangle^2)$	0.0002
Averaged local Kolmogorov scale $\eta_k = (\nu^3/\epsilon)^{1/4}$	0.07 mm
PIV neighboring vector distance δ_v	0.86 mm $\simeq 12\eta_k$
Schmidt number Sc	500−700
Averaged local Batchelor scale $\eta_b = \eta_k/\sqrt{\mathrm{Sc}}$	0.003 mm
PLIF pixel resolution δ_θ	0.054 mm $\simeq 18\eta_b$
Inertial subrange	$(15\delta_v - 35\delta_v) \simeq (185\eta_k - 430\eta_k)$

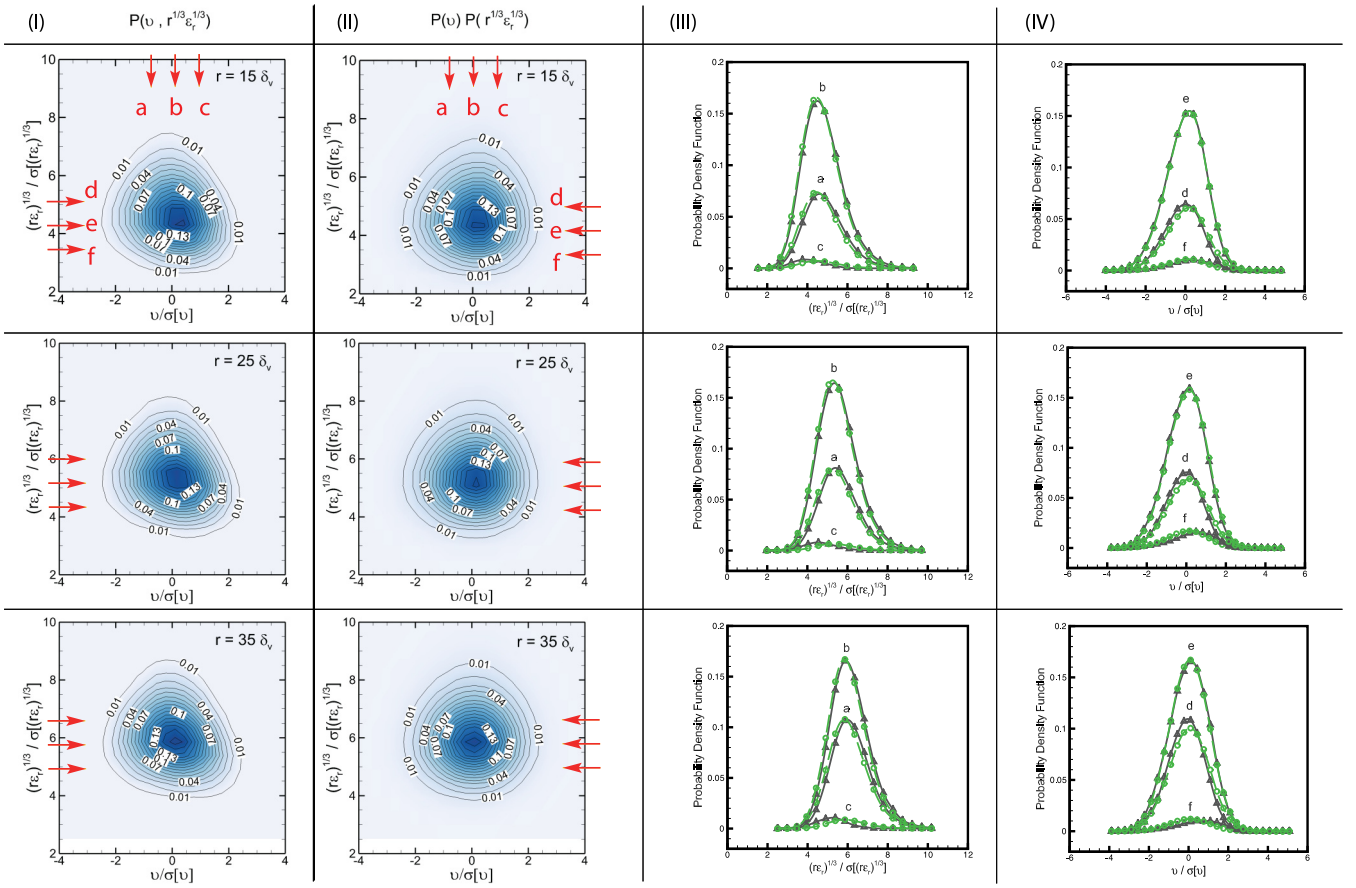

FIG. 4. (Color online) Comparison of PDFs at different r's in the inertial subrange, from left to right: (I) $P(\upsilon,(r\epsilon_r)^{1/3})$ and (II) $P(\upsilon)P((r\epsilon_r)^{1/3})$. Both axes are normalized by their corresponding standard deviations. (III) Profiles of $P(\upsilon,(r\epsilon_r)^{1/3})$ and $P(\upsilon)P((r\epsilon_r)^{1/3})$ at *a, b, c*. (IV) Profiles of $P(\upsilon,(r\epsilon_r)^{1/3})$ and $P(\upsilon)P((r\epsilon_r)^{1/3})$ at *d, e, f*. Gray circles and solid lines: $P(\upsilon,(r\epsilon_r)^{1/3})$; green triangles and dashed lines: $P(\upsilon)P((r\epsilon_r)^{1/3})$.

consecutive frames along the streamwise direction have been recorded, and the field of view for each frame is 11×11 cm^2. A sample pair of snapshots of the velocity field combined with the scalar field on a 128×128 grid are shown in Fig. 1. The mean streamwise velocity and scalar distributions are shown in Fig. 2, calculated from 600 snapshots, where $\theta(x,y) = \Delta\rho(x,y)/\Delta\rho_0$ is the nondimensional scalar ($0 \leqslant \theta \leqslant 1$). In this study, data from a downstream region of 3.5×8.6 cm^2 (enclosed by red dashed lines in Fig. 2, centered at $x/D \simeq 20$, $y/D = 0$) are selected from each snapshot, where the flow is fully developed. A total of 2.4 mega data points are used for the statistical analysis presented in this study.

As suggested in Ref. [18], as many of the measurable elements of s_{ij} should be applied to reduce the overintermittent behavior. Thus, in this study, four elements resolved from 2D PIV are applied to calculate ϵ by

$$\epsilon \simeq \nu \left[4\left(\frac{\partial u_1'}{\partial x_1}\right)^2 + 4\left(\frac{\partial u_2'}{\partial x_2}\right)^2 + 4\frac{\partial u_1'}{\partial x_1}\frac{\partial u_2'}{\partial x_2} + 3\left(\frac{\partial u_1'}{\partial x_2}\right)^2 + 3\left(\frac{\partial u_2'}{\partial x_1}\right)^2 + 6\frac{\partial u_1'}{\partial x_2}\frac{\partial u_2'}{\partial x_1} \right], \quad (8)$$

where the local isotropy assumption for unresolved terms of s_{ij} is applied. See details in Ref. [32]. The central difference scheme is applied to compute s_{ij}. A one-dimensional (along the streamwise direction) average of ϵ is applied to obtain ϵ_r, i.e.,

$$\epsilon_r = \frac{1}{N+1}\sum_{j=0}^{N} \epsilon(x_1 + j\delta_v, x_2), \quad (9)$$

where $N = r/\delta_v$.

In previous experimental tests of RSH, the scalar dissipation is estimated using the assumption of isotropic. However, similar to the estimate of energy dissipation, as many measurable elements as possible should be used to reduce the overintermittent (or underintermittent) behavior. Therefore in this study, an assumption is applied to calculate χ by

$$\chi = 2\Gamma\left[\left(\frac{\partial\theta'}{\partial x_1}\right)^2 + 2\left(\frac{\partial\theta'}{\partial x_2}\right)^2\right], \quad (10)$$

as used in Refs. [33,34]. One is reminded that $\partial\theta'/\partial x_j$ is calculated using PLIF data, which is of a spatial resolution of $\Delta_\theta = 0.054$ mm $= 18\eta_b$ before the data of the scalar field is sampled to match the spatial resolution of the velocity field.

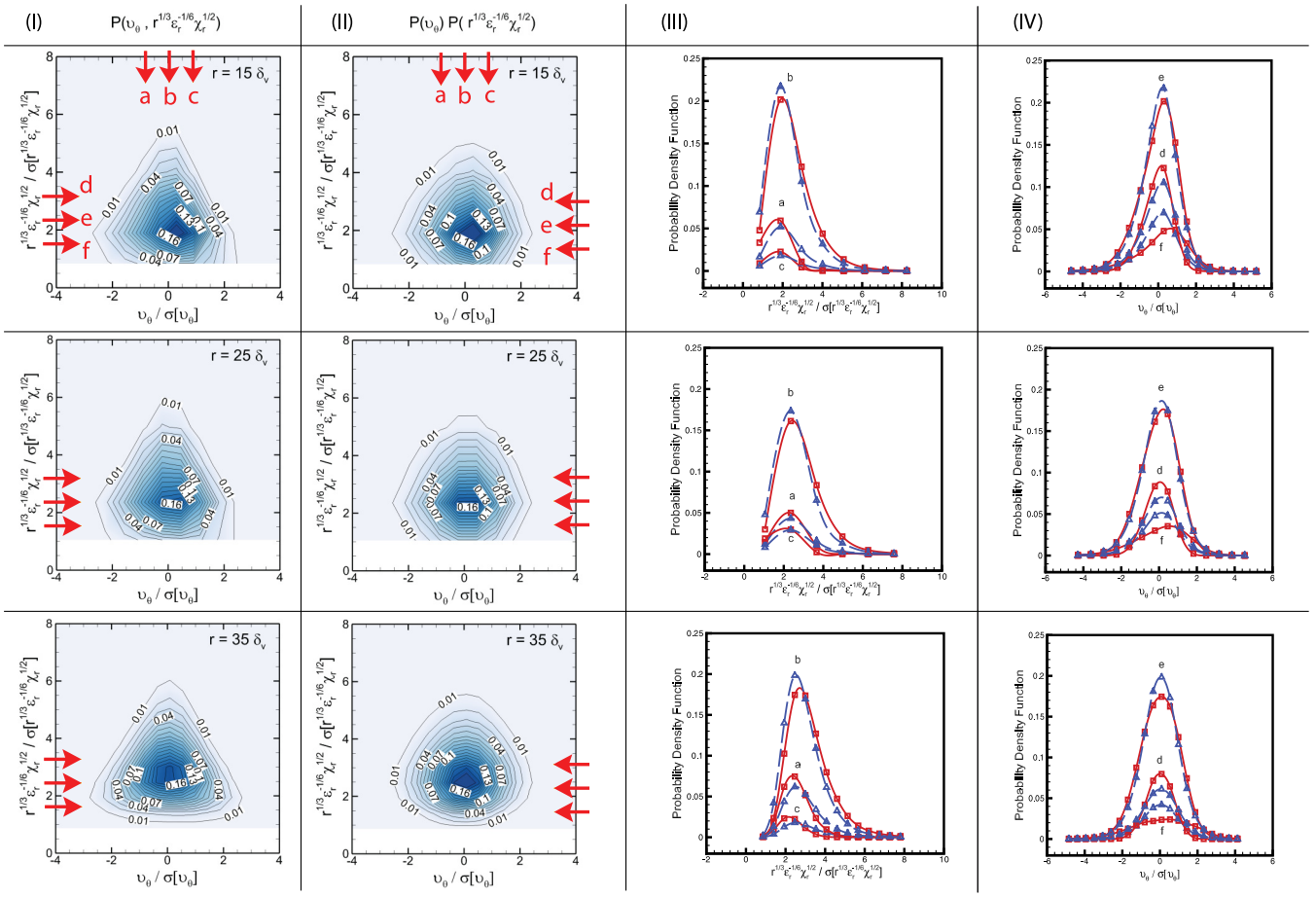

FIG. 5. (Color online) Comparison of PDFs at different r's in the inertial subrange, from left to right: (I) $P(\upsilon_\theta, r^{1/3}\epsilon_r^{-1/6}\chi_r^{1/2})$ and (II) $P(\upsilon_\theta)P(r^{1/3}\epsilon_r^{-1/6}\chi_r^{1/2})$. Both axes are normalized by their corresponding standard deviations. (III) Profiles of $P(\upsilon_\theta, r^{1/3}\epsilon_r^{-1/6}\chi_r^{1/2})$ and $P(\upsilon_\theta)P(r^{1/3}\epsilon_r^{-1/6}\chi_r^{1/2})$ at *a, b, c*. (IV) Profiles of $P(\upsilon_\theta, r^{1/3}\epsilon_r^{-1/6}\chi_r^{1/2})$ and $P(\upsilon_\theta)P(r^{1/3}\epsilon_r^{-1/6}\chi_r^{1/2})$ at *d, e, f*. Red squares and solid lines: $P(\upsilon_\theta, r^{1/3}\epsilon_r^{-1/6}\chi_r^{1/2})$; blue triangles and dashed lines: $P(\upsilon_\theta)P(r^{1/3}\epsilon_r^{-1/6}\chi_r^{1/2})$.

Similar to ϵ_r, χ_r is obtained by

$$\chi_r = \frac{1}{N+1}\sum_{j=0}^{N}\chi(x_1 + j\delta_v, x_2). \tag{11}$$

To obtain υ and υ_θ, $\Delta u_r'$ and $\Delta\theta_r'$, as defined previously, are calculated along the streamwise direction, as commonly used in previous studies.

III. RESULT AND DISCUSSION

The independence of υ on r and ϵ_r and that of υ_θ on r, ϵ_r, and χ_r are examined through using JPDF and PDF. If the independence exists, one should have $P(\upsilon, (r\epsilon_r)^{1/3}) = P(\upsilon)P((r\epsilon_r)^{1/3})$ and $P(\upsilon_\theta, r^{1/3}\epsilon_r^{-1/6}\chi_r^{1/2}) = P(\upsilon_\theta)P(r^{1/3}\epsilon_r^{-1/6}\chi_r^{1/2})$ [21]. In Fig. 4, although the outer region of those PDF contours displays certain differences, the central regions demonstrate strong similarities at different r's. For better illustration, as marked in Fig. 4, the profiles of the 2D PDFs are selected at different sections across *a, b, c* and *d, e, f* from both $P(\upsilon, r^{1/3}\epsilon_r^{1/3})$ and $P(\upsilon)P(r^{1/3}\epsilon_r^{1/3})$. In Fig. 4, at all three characteristic r's, the gray curves [indicating $P(\upsilon, r^{1/3}\epsilon_r^{1/3})$] nearly coincide with the green curves [indicating $P(\upsilon)P(r^{1/3}\epsilon_r^{1/3})$]. Thus, υ has independence upon r and ϵ_r. The degree of independence in the outer regions is yet improved than the one in Ref. [21].

The test of independence behavior of υ_θ is shown in Fig. 5, where the central regions of those contours demonstrate similarities to a certain extent, but the outer regions yield more differences at different r's. In Fig. 5, the red curves [indicating $P(\upsilon_\theta, r^{1/3}\epsilon_r^{-1/6}\chi_r^{1/2})$] have distinct differences from the blue curves [indicating $P(\upsilon_\theta)\ P(r^{1/3}\epsilon_r^{-1/6}\chi_r^{1/2})$]. Thus, the independence of υ_θ on r, ϵ_r, and χ_r is not sufficiently supported, i.e., it is difficult to determine the existence of the independence with strong confidence. Therefore, a further examination of the second order moments of υ and υ_θ is conducted: If the independence exists, the averages of υ^2 obtained by $\langle \Delta u_r^2/(r\epsilon_r)^{2/3}\rangle$ should be equal to those obtained by $\langle \Delta u_r^2\rangle/\langle (r\epsilon_r)^{2/3}\rangle$, and the same to averages of υ_θ^2. In Fig. 6, $\langle \upsilon^2\rangle$ from the two methods are nearly coincident (ratio $\sim$0.95) over the inertial subrange. However, $\langle \upsilon_\theta^2\rangle$ from the two methods show a large difference (ratio between 0.61 and 0.68). One is reminded that the uncertainties of measurements are also plotted in Fig. 6, although they are small. These observations suggest that the independence of υ on r and ϵ_r exists in the inertial subrange, while that of υ_θ on r, ϵ_r, and χ_r is not clearly observed.

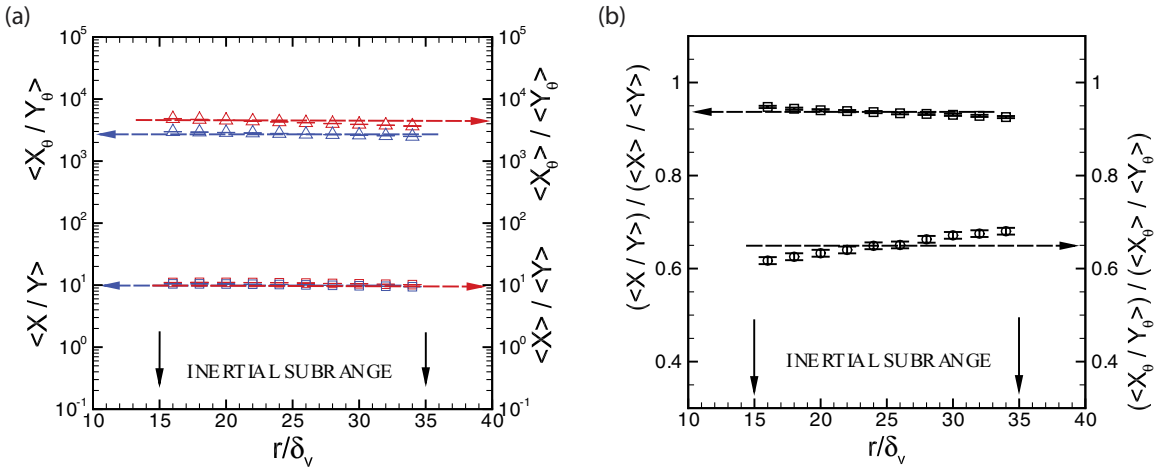

FIG. 6. (Color online) (a) $\langle \Delta u_r^2/(r\epsilon_r)^{2/3}\rangle$ and $\langle \Delta u_r^2\rangle/\langle(r\epsilon_r)^{2/3}\rangle$, as well as $\langle \Delta\theta_r^2/(r^{1/3}\epsilon_r^{-1/6}\chi_r^{1/2})^2\rangle$ and $\langle \Delta\theta_r^2\rangle/\langle(r^{1/3}\epsilon_r^{-1/6}\chi_r^{1/2})^2\rangle$. (b) $\langle \Delta u_r^2/(r\epsilon_r)^{2/3}\rangle/(\langle \Delta u_r^2\rangle/\langle(r\epsilon_r)^{2/3}\rangle)$ and $\langle \Delta\theta_r^2/(r^{1/3}\epsilon_r^{-1/6}\chi_r^{1/2})^2\rangle/(\langle \Delta\theta_r^2\rangle/\langle(r^{1/3}\epsilon_r^{-1/6}\chi_r^{1/2})^2\rangle)$. [$X = \Delta u_r^2$, $Y = (r\epsilon_r)^{2/3}$, $X_\theta = \Delta\theta_r^2$, and $Y_\theta = (r^{1/3}\epsilon_r^{-1/6}\chi_r^{1/2})^2$.] Vertical bars represent the uncertainties of measurements obtained from error propagation.

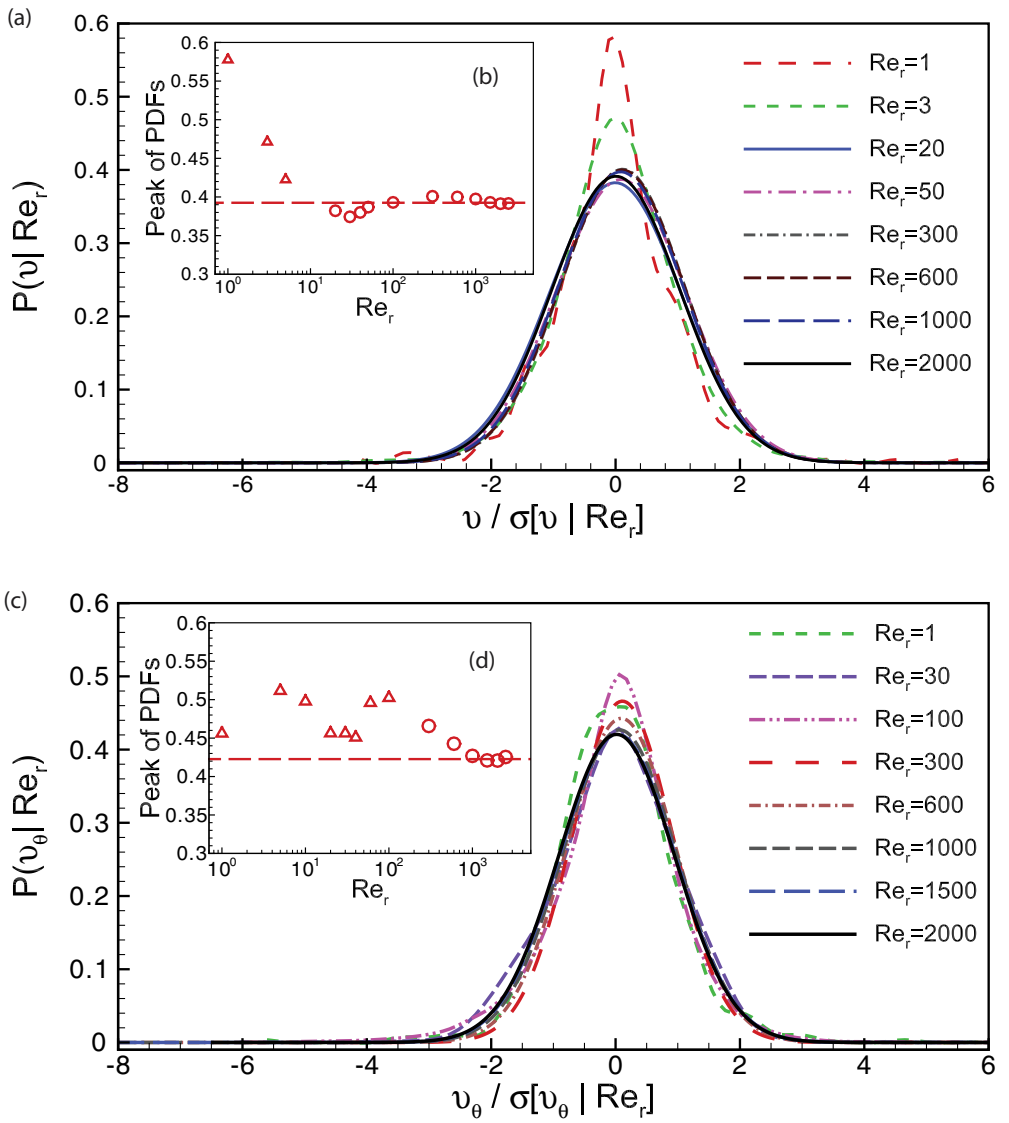

FIG. 7. (Color online) Conditional PDFs: (a) $P(\upsilon|\mathrm{Re_r})$ and (c) $P(\upsilon_\theta|\mathrm{Re_r})$. Circles in insets (b), (d) show peaks of Gaussian curves, and triangles in insets (b), (d) show peaks of non-Gaussian distributions.

To test the second and third hypotheses in RSH, the PDF of υ conditioned on $\mathrm{Re_r}$, $P(\upsilon|\mathrm{Re_r})$, needs to be examined [21]. As shown in Fig. 7, for small $\mathrm{Re_r}$ (e.g., $\mathrm{Re_r} = 1,3,5$), the PDFs cannot be described by Gaussian distributions. For larger $\mathrm{Re_r}$, $P(\upsilon|\mathrm{Re_r})$ have strong Gaussian distributions. All Gaussian curves collapse when $\mathrm{Re_r} > 100$, suggesting $\mathrm{Re_r}$ independence of $P(\upsilon|\mathrm{Re_r})$. Similar results are also observed for the conditional PDF of υ_θ conditioned on $\mathrm{Re_r}$ [$P(\upsilon_\theta|\mathrm{Re_r})$], but the Gaussian curves of $P(\upsilon_\theta|\mathrm{Re_r})$ collapse when $\mathrm{Re_r} > 1000$ [rather than 100 for $P(\upsilon|\mathrm{Re_r})$]. Another finding is that the peaks of PDFs, as $\mathrm{Re_r}$ increases, experience oscillations before converging to a value of about 0.39 for $P(\upsilon|\mathrm{Re_r})$ and 0.42 for $P(\upsilon_\theta|\mathrm{Re_r})$ in the insets, where the non-Gaussian and Gaussian peaks are marked by triangles and circles, respectively. These oscillations need to be further investigated for smaller $\mathrm{Re_r}$.

Furthermore, in the previous hot-cold-wire probe tests of RSH (and RSH-P), the bimodal behavior of PDFs exists when r is small (see Figs. 10–13 in Ref. [21]). Besides, strong oscillations can be also observed [from Figs. 10–13 in Ref. [21] (shown in log scale)]. However, no bimodal behavior of PDFs and oscillations are observed in our testing results (as shown in Fig. 7).

IV. CONCLUSION

Previous experimental tests of refined similarity hypotheses were usually performed in a wind tunnel by applying hot-cold-wire probes. Taylor's hypothesis has to be applied to convert the temporal series of data into spatial series of data, however, Taylor's hypothesis is believed to bring in possible errors to the test of RSH (and RSH-P) [14,15,24–26]. In this study, the simultaneous obtained high-resolution velocity and scalar fields are used to test RSH and RSH-P without adopting Taylor's hypothesis. For RSH, the results show that the stochastic variable υ is independent of r and ϵ_r in the inertial subrange. $P(\upsilon|\mathrm{Re_r})$ experience non-Gaussian distribution when $\mathrm{Re_r}$ is small, however, when $\mathrm{Re_r}$ increases, $P(\upsilon|\mathrm{Re_r})$ shows a Gaussian distribution. Investigating $P(\upsilon|\mathrm{Re_r})$ strongly supports the statement that $P(\upsilon)$ is independent on $\mathrm{Re_r}$ when $\mathrm{Re_r} > 100$. We also observe $\mathrm{Re_r}$ dependence of $P(\upsilon)$ when $\mathrm{Re_r} \sim 1$. In addition, the oscillation of the converging of $P(\upsilon|\mathrm{Re_r})$ is observed. For RSH-P, $P(\upsilon_\theta)$ depends on $\mathrm{Re_r}$ when $r \ll L$ and is universal when $\mathrm{Re_r} \gg 1$. However, the independence of υ_θ on r, ϵ_r, and χ_r is not sufficiently supported with strong confidence by the present experimental results. In addition, the bimodal behavior of PDFs and strong oscillations exist in the previous experimental testing results when r is small. However, no bimodal behavior of PDFs and oscillations are observed in our testing results.

ACKNOWLEDGMENTS

The authors are grateful to two anonymous reviewers for their helpful comments and constructive suggestions.

[1] L. F. Richardson, *Weather Prediction by Numerical Process* (Cambridge University Press, Cambridge, UK, 1922).
[2] A. Kolmogorov, Dokl. Akad. Nauk SSSR **30**, 301 (1941).
[3] A. D. Staicu, *Intermittency in Turbulence* (University of Technology, Eindhoven, 2002).
[4] S. B. Pope, *Turbulent flows* (Cambridge University Press, Cambridge, UK, 2001).
[5] A. Kolmogorov, J. Fluid Mech. **13**, 82 (1962).
[6] A. Oboukhov, J. Fluid Mech. **13**, 77 (1962).
[7] I. Hosokawa and K. Yamamoto, J. Phys. Soc. Jpn. **60**, 1852 (1991).
[8] I. Hosokawa and K. Yamamoto, Phys. Fluids A **4**, 457 (1992).
[9] G. Stolovitzky, P. Kailasnath, and K. Sreenivasan, Phys. Rev. Lett. **69**, 1178 (1992).
[10] A. A. Praskovsky, Phys. Fluids A **4**, 2592 (1992).
[11] S. Thoroddsen and C. V. Atta, Phys. Fluids A **4**, 2592 (1992).
[12] S. Chen, G. Doolen, R. Kraichnan, and Z.-S. She, Phys. Fluids A **5**, 458 (1993).
[13] G. Stolovizky and K. Sreenivasan, Rev. Mod. Phys. **66**, 229 (1994).
[14] S. Thoroddsen, Phys. Fluids **7**, 691 (1995).
[15] S. Chen, G. D. Doolen, R. H. Kraichnan, and L.-P. Wang, Phys. Rev. Lett. **74**, 1755 (1995).
[16] A. Praskovasky, E. Praskovaskaya, and T. Horst, Phys. Fluids **9**, 2465 (1997).
[17] I. Hosokawa, S. Oide, and K. Yamamoto, Phys. Rev. Lett. **77**, 4548 (1996).
[18] S. Almalkie and S. M. de Bruyn Kops, J. Fluid Mech. **697**, 204 (2012).
[19] I. Hosokawa, Phys. Rev. E **49**, 4775 (1994).
[20] R. A. Antonia and C. W. V. Atta, Phys. Fluids **17**, 1776 (1974).
[21] Y. Zhu, R. Antonia, and I. Hosokawa, Phys. Fluids **7**, 1637 (1995).
[22] G. Stolovitzky, P. Kailasnath, and K. Sreenivasan, J. Fluid Mech. **297**, 275 (1995).
[23] L. Wang, S. Chen, and J. G. Brasseur, J. Fluid Mech. **400**, 163 (1999).
[24] W. J. A. Dahm and K. B. Southerland, Phys. Fluids **9**, 2101 (1997).
[25] J. C. D. Álamo and J. Jiménez, J. Fluid Mech. **640**, 5 (2009).
[26] P. Moin, J. Fluid Mech. **640**, 1 (2009).
[27] P. V. Vukoslavčević, I. M. Radulović, and J. M. Wallace, Exp. Fluids **39**, 703 (2005).
[28] P. K. Yeung, S. B. Pope, and B. L. Sawford, J. Turbul. **7**, 1 (2006).
[29] T. Ishihara, Y. Kaneda, M. Yokokawa, K. Itakura, and A. Uno, J. Fluid Mech. **592**, 335 (2007).
[30] T. Ishihara, T. Gotoh, and Y. Kaneda, Annu. Rev. Fluid Mech. **41**, 165 (2009).
[31] D. Xu and J. Chen, Exp. Fluids **53**, 145 (2012).
[32] P. Doron, L. Bertuccioli, J. Katz, and T. Osborn, J. Phys. Oceanogr. **31**, 2108 (2001).
[33] F. Anselmet and R. A. Antonia, Phys. Fluids **28**, 1048 (1985).
[34] Z. Hao, T. Zhou, Y. Zhou, and J. Mi, Exp. Fluids **44**, 279 (2008).